Chemical Physics Letters 541 (2012) 110–116

Contents lists available at SciVerse ScienceDirect

Chemical Physics Letters

journal homepage: www.elsevier.com/locate/cplett

Absorption and fluorescence spectra of the neutral and anionic green fluorescent protein chromophore: Franck–Condon simulation

Tsung-wei Huang [a], Ling Yang [a,b], Chaoyuan Zhu [a,*], Sheng Hsien Lin [a]

[a] Department of Applied Chemistry, Institute of Molecular Science and Center for Interdisciplinary Molecular Science, National Chiao-Tung University, Hsinchu 30050, Taiwan
[b] Institute of Theoretical and Simulation Chemistry, Academy of Fundamental and Interdisciplinary Science, Harbin Institute of Technology, Harbin 150080, PR China

ARTICLE INFO

Article history:
Received 27 February 2012
In final form 16 May 2012
Available online 26 May 2012

ABSTRACT

Absorption and fluorescence spectra of the neutral and anionic green fluorescent protein (GFP) chromophore, namely *p*-hydroxybenzylideneimidazolidinone (*p*-HBDI), have been simulated using the Franck–Condon factors including inhomogeneous broadening of solvent effect. Ground and the first excited states were calculated by time dependent density functional theory with and without the polarizable continuum model environment. Simulated peak of the neutral/anionic *p*-HBDI at 380 nm (423 nm)/421 nm agrees with experiment value 370 nm (434 nm)/419 nm for absorption (fluorescence) spectrum. Simulated width of the neutral/anionic *p*-HBDI at 0.51 eV (0.54 eV)/0.57 eV agrees with experiment value 0.54 eV (0.66 eV)/0.56 eV for absorption (fluorescence) spectrum.

1. Introduction

The discovery of the green fluorescent protein (GFP) led to a new revolution in molecular biology since the middle of the 20th century, and absorption and fluorescence spectra of GFP have been widely studied on the molecular level from both theory and experiment. GFP consists of 238 amino acids and its crystal structure was determined as an 11-stranded β-barrel [1,2]. The GFP chromophore absorbs light energy of a specific wavelength and then re-emits light as fluorescence at a longer wavelength. Primary structure of the GFP chromophore is *p*-hydroxybenzylideneimidazolinone (*p*-HBDI, see Figures 1 and 2) that is formed from tripeptide Serine-65 (Ser65), Tyrosine-66 (Tyr66), and Glycine-67 (Gly67) in the native protein [3,4]. GFP variants may be classified as several classes based on the difference of their chromophores; there are wild-type mixture of neutral phenol and anionic phenolate, phenolate anion, neutral phenol, and so on [5]. The wild-type GFP (wt-GFP) has two characteristic absorption bands at room-temperature; one is a major excitation peak at about 395 nm from the neutral chromophore and another minor peak is at about 475 nm ascribed to excitation of the anionic chromophore [5–11]. The equilibrium between these two forms is influenced by external factors like temperature, PH, and the protein environment [2,12]. In order to understand a relative contribution of the neutral and anionic form of the *p*-HBDI chromophore, many studies have been carried out to show the influence of the acid–base properties and the solvatochromic behavior on its absorption and fluorescence spectra [13–17]. In the present study, we have introduced inhomogeneous broadening in Franck–Condon simulation [18–21] to treat spectra of the neutral and anionic *p*-HBDI in solution. We have calculated equilibrium geometries of both ground and the first excited states of neutral and anionic *p*-HBDI without and with solvent effect, namely the polarizable continuum model (PCM) [22], by DFT and time dependent density functional theory (TD-DFT). The combination of PCM and TDDFT methods has been widely used for computing electronic structure in the presence of solvent effect [22–24]. However, the interaction between vibronic excited state of molecule and solvent is key influence to molecular spectrum and this interaction is taken into account by inhomogeneous broadening approach in the present study.

2. Computational details

All calculations were carried out using Gaussian 09 program package [25]. A primary test calculation was done with both C_1 and C_s group symmetry for both ground state S_0 and the first excited state S_1. The results show that the imidazolidinone and phenol rings are almost in the same plane for these two types of symmetry, and difference is mainly in orientation of the two methyl groups attached to the imidazolidinone ring. An analysis of spectroscopy calculation proved that the C_1 group symmetry is correct. Equilibrium geometries of S_0 and S_1 states were calculated by density functional theory DFT and time-dependent DFT (TD-DFT) with the same basis set B3LYP/6-31+G(d), respectively without and with PCM condition.

Within displaced harmonic oscillator approximation, absorption and fluorescence coefficients can be analytically derived as follows [19,21]:

* Corresponding author. Fax: +886 3 5723764.
E-mail address: cyzhu@mail.nctu.edu.tw (C. Zhu).

0009-2614/$ - see front matter © 2012 Elsevier B.V. All rights reserved.
http://dx.doi.org/10.1016/j.cplett.2012.05.039

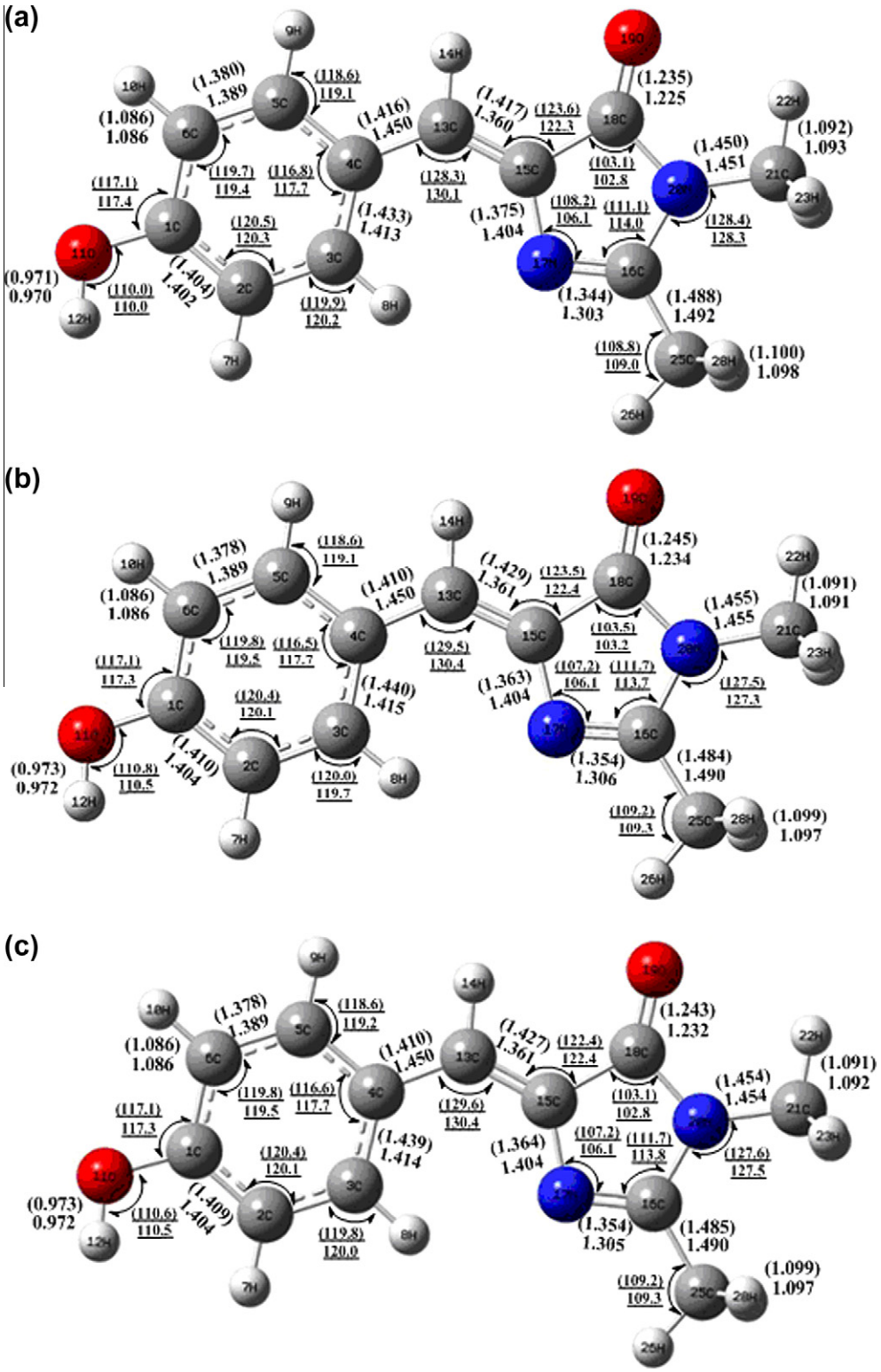

Figure 1. Optimized geometries of the S_0 and S_1 states for the neutral *p*-HBDI using B3LYP/6-31+G(d) and TD-B3LYP/6-31+G(d), respectively; (a) without PCM, (b) with PCM in methanol solvent and (c) with PCM in THF solvent. The bond lengths in angstrom and angles in degree (parameters in the brackets for S_1, otherwise for S_0).

$$\langle\alpha(\omega)\rangle \propto \omega \int_{-\infty}^{\infty} dt \exp\left[it(\omega_{ba}-\omega) - \frac{D_{ba}^2 t^2}{4} - \gamma_{ba}|t| - \sum_j S_j\{(2\bar{n}_j+1) - (\bar{n}_j+1)e^{it\omega_j} - \bar{n}_j e^{-it\omega_j}\}\right] \quad (1)$$

and

$$\langle I(\omega)\rangle \propto \omega^3 \int_{-\infty}^{\infty} dt \exp\left[-it(|\omega_{ba}|-\omega) - \frac{D_{ba}^2 t^2}{4} - \gamma_{ba}|t| - \sum_j S_j\{(2\bar{n}_j+1) - (\bar{n}_j+1)e^{it\omega_j} - \bar{n}_j e^{-it\omega_j}\}\right] \quad (2)$$

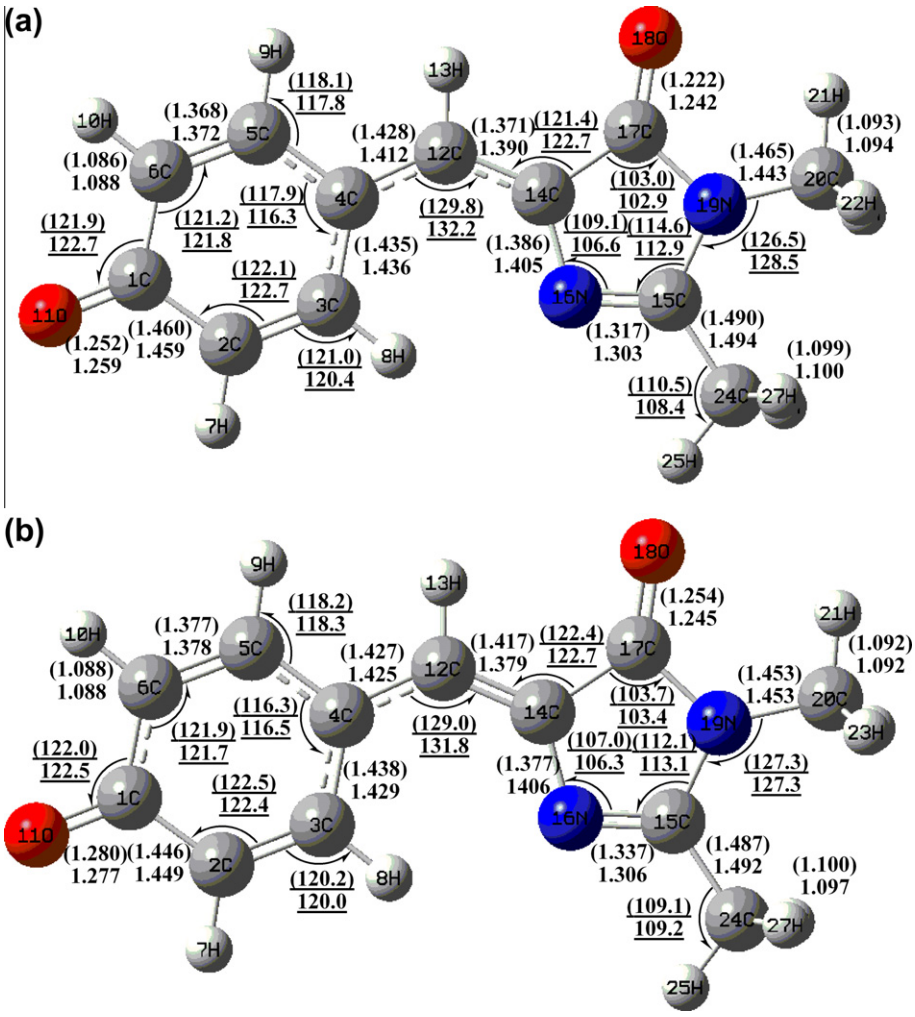

Figure 2. Optimized geometries of the S_0 and S_1 states for the anionic *p*-HBDI using B3LYP/6-31+G(d) and TD-B3LYP/6-31+G(d), respectively; (a) without PCM and (b) with PCM in methanol solvent. The bond lengths in angstrom and angles in degree (parameters in the brackets for S_1, otherwise for S_0).

where ω_{ba} represents electronically adiabatic excitation energy between electronic states *b* and *a*. $\bar{n}_j = (e^{\hbar\omega_j/k_BT} - 1)^{-1}$is the average phonon distribution and γ_{ba} represents the homogeneous broadening parameter. D_{ba} represents inhomogeneous broadening parameter that reflects dynamic interaction between vibronic excited states of molecule and solvent, and ω_j is the *j*-th normal mode vibrational frequency. The Huang–Rhys factor S_j corresponding to the *j*-th normal mode is defined as

$$S_j = \frac{1}{2\hbar}\omega_j d_j^2 \tag{3}$$

where displacement d_j is given by

$$d_j = Q'_j - Q_j = \sum_n L_{jn}(q'_n - q_n) \tag{4}$$

The q'_n and q_n in Eq. (4) are the mass-weighted Cartesian coordinates at equilibrium geometries of the electronic excited and ground states, respectively. Transformation matrix *L* in Eq. (4) can be computed with frequency analysis using G09 programs.

3. Results and discussions

Figure 1 shows the methyl-terminated neutral model chromophore (*p*-HBDI) in the wt-GFP. Figure 1a shows the optimized geometries without PCM condition in which the bond lengths and angles in the S_0 and S_1 states are very similar for the phenol ring. The bridge bonds 4C−13C and 13C−15C are single and double bonds, respectively for both S_0 and S_1 states; 4C−13C single bond is slightly shorten and 13C−15C double bond is slightly stretched from S_0 to S_1 state, and 4C−13C−15C bridge angle is reduced from 130.1° to 128.3°. It is also shown that from S_0 to S_1 states the 16C−17N bond is expanded by 0.04 Å, while 17N−16C−20N angle in the imidazolidinone ring is reduced 3°. The other differences are about 0.001–0.035 Å for bond lengths and 0.3°–2.1° for angles. These results are in line with the other calculations reported by Helms et al. and Polyakov et al. [26,27]. Figure 1b shows the optimized geometries with PCM condition in methanol (CH_3OH, dielectric constant ε = 32.61) in which the bridge bonds are almost same as those of calculation without PCM conditions, and only bridge angle 4C−13C−15C is reduced from 130.4° to 129.5°. Figure 1c shows the optimized geometries with PCM condition in THF (C_4H_8O, dielectric constant ε = 7.43) in which the bridge bonds show very slight changes in comparison with the results in Figure 1a and only bridge angle 4C−13C−15C is reduced from 130.4° to 129.6°. It is basically quite similar for equilibrium geometries calculated with and without PCM condition.

Figure 2 shows the methyl-terminated anionic model chromophore (*p*-HBDI) in the wt-GFP. Figure 2a shows the optimized geometries without PCM condition in which the bond lengths and angles in the S_0 and S_1 states are also very similar for the

Table 1
Calculated adiabatic 0–0 excitation energies, and vibrational frequencies (in units of cm^{-1}) for the ground state by B3LYP/6-31+G(d) and its corresponding Huang–Rhys factors (dimensionless vibronic coupling).

Without PCM			PCM (methanol)			PCM (THF)		
Neutral p-HBDI								
3.1 eV (399 nm)			2.74 eV (452 nm)			2.8 eV (443 nm)		
Mode	Freq	S^{HR}	Mode	Freq	S^{HR}	Mode	Freq	S^{HR}
ν_{16}	1627	0.2353	ν_{16}	1621	0.4082	ν_{16}	1622	0.3511
ν_{29}	1351	0.1352	ν_{29}	1348	0.2489	ν_{29}	1349	0.2228
ν_{32}	1261	0.1197	ν_{32}	1261	0.1682	ν_{32}	1262	0.1533
ν_{40}	1049	0.1940	ν_{40}	1048	0.1463	ν_{40}	1048	0.1493
ν_{42}	1019	0.1725	ν_{42}	1025	0.1549	ν_{42}	1024	0.1725
ν_{53}	720	0.4103	ν_{53}	719	0.3590	ν_{53}	719	0.3441
ν_{60}	517	0.2034	ν_{60}	516	0.2794	ν_{60}	516	0.2355
ν_{66}	337	0.1240	ν_{66}	338	0.1823	ν_{66}	338	0.1577
ν_{76}[a]	80	0.0679	ν_{75}	79	0.1198	ν_{75}	79	0.0977
Anionic p-HBDI								
2.81 eV (441 nm)			2.58 eV (480 nm)					
Mode	Freq	S^{HR}	Mode	Freq	S^{HR}			
ν_{29}[b]	1319	0.3672	ν_{17}[b]	1523	0.5218			
ν_{32}[b]	1202	0.4230	ν_{28}[b]	1348	0.3841			
ν_{38}[b]	1050	0.7453	ν_{30}[b]	1288	0.3253			
ν_{44}[c]	930	0.5756	ν_{39}[c]	1023	0.3215			
ν_{55}[c]	604	0.2017	ν_{51}[c]	723	0.3418			
ν_{64}[c]	276	0.7648	ν_{54}[c]	633	0.2398			
ν_{65}[c]	247	0.3368	ν_{58}[c]	514	0.3299			
			ν_{60}[c]	455	0.3223			
			ν_{63}[c]	337	0.4184			
			ν_{72}[c]	78	0.3806			

[a] This vibration mode is equal to number 75 in methanol and THF solvents.
[b] Vibration modes unrelated with oxygen atoms.
[c] Vibration modes related to oxygen atoms.

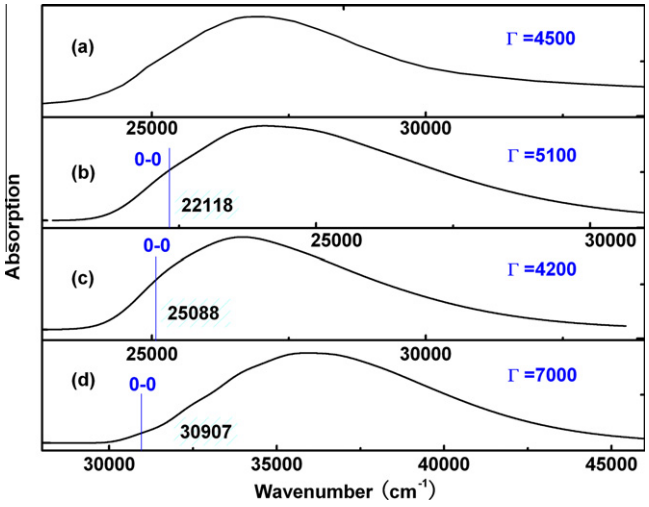

Figure 3. Absorption spectra of the neutral *p*-HBDI measured and calculated at temperature $T = 298$ K. Vertical bars stand for adiabatic 0–0 excitation energy positions and Γ for spectral widths. Homogeneous and inhomogeneous broadening parameters are chosen as 10 cm^{-1} and 800 cm^{-1} in Franck–Condon simulation. (a) Experiment data from Ref. [15]; (b) with PCM in methanol solvent and (c) without PCM (equilibrium geometries calculated from B3LYP and TD-B3LYP); (d) without PCM (equilibrium geometries calculated from HF and CIS methods).

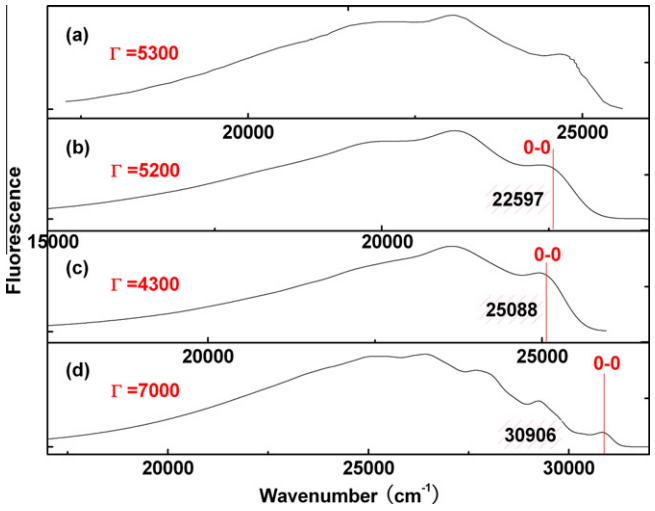

Figure 4. Fluorescence spectra of the neutral *p*-HBDI measured and calculated at temperature $T = 77$ K. Vertical bars stand for adiabatic 0–0 excitation energy positions and Γ for spectral widths. Homogeneous and inhomogeneous broadening parameters are chosen as 10 cm^{-1} and 400 cm^{-1} in Franck–Condon simulation. (a) Experiment data from Ref. [16]; (b) with PCM in methanol solvent and (c) without PCM (equilibrium geometries calculated from B3LYP and TD-B3LYP); (d) without PCM (equilibrium geometries calculated from HF and CIS method).

phenol ring. The bridge bonds 4C–12C and 12C–14C are conjugate bonds for S_0 state and conjugate and double bonds for S_1 state; 4C–12C conjugate bond is slightly elongated and 12C–14C conjugate bond is shortened from S_0 to S_1, and bridge angle 4C–12C–14C is reduced from 132.2° to 129.8°. It is also shown that the 15C–16N bond and 16N–15C–19N angle in the imidazolidinone ring are expanded by 0.014 Å and 1.7° from S_0 to S_1 state, respectively. The other differences are about 0.001–0.022 Å for bond lengths and 0.1–2.5° for angles. These results are very similar to other calculations reported by Helms et al. [26], Polyakov et al. [27], and Olsen and Smith [28,29]. Figure 2b shows the optimized geometries with PCM condition in methanol (CH_3OH, dielectric constant $\varepsilon = 32.61$) in which the bridge conjugate bond 4C–12C and 12C–14C double bond are elongated from S_0 to S_1; and the

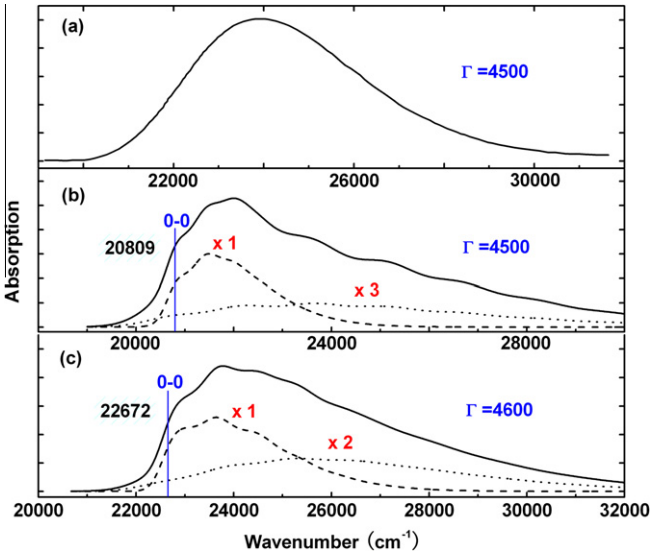

Figure 5. Absorption spectra of the anionic *p*-HBDI measured and calculated at temperature $T = 298$ K. Vertical bars stand for adiabatic 0–0 excitation energy positions and Γ for spectral widths. Homogeneous parameter is chosen as 10 cm^{-1} and inhomogeneous broadening parameters are chosen as 350 cm^{-1} and 800 cm^{-1} for vibration modes related and irrelated to oxygen atoms in Franck–Condon simulation, respectively. (a) Experiment data from Ref. [16], (b) with PCM in methanol solvent and (c) without PCM (equilibrium geometries calculated from B3LYP and TD-B3LYP for S_0 and S_1 states, solid). Spectra of the vibrations related to oxygen atoms (dashed lines) and spectra of the vibrations unrelated to oxygen atoms (dotted lines).

bridge angle 4C−12C−14C is the same as it is shown in Figure 2a for the calculation without PCM condition. The present calculations agree well with Garavelli and Negri's results [30]. However, for the anionic chromophore it is quite different for equilibrium geometries calculated with and without PCM condition.

Next, we have carried out frequency calculations for the equilibrium geometries of neutral/anionic S_0 and S_1 states, and all 78/75 vibrational normal-mode frequencies are positive (this means that we got correct local minima for S_0 and S_1 states). Only nine/seven (nine/ten) normal modes out of 78/75 without PCM (with PCM in methanol) shown in Table 1 play important role for spectra with significant figures of vibronic couplings expressed in terms of Huang–Rhys factors (S^{HR}), and its magnitudes vary from 0.24/0.76 to 0.07/0.20 for the neutral/anionic *p*-HBDI geometries calculated without PCM (see Figures 1a and 2a), and from 0.4/0.52 to 0.12/0.24 for the geometries calculated with PCM in methanol (see Figures 1b and 2b), respectively. The distributions of these nine Huang–Rhys factors for the neutral *p*-HBDI are basically similar for the equilibrium geometries calculated without and with PCM condition, and this means that the profiles of spectra would be similar too (see Figures. 3 and 4); while the Huang–Rhys factor distributions for the anionic *p*-HBDI are quite different for the equilibrium geometries calculated without and with PCM condition, and this implies that the profiles of spectra would be different too (seen in Figure 5). We have computed adiabatic excitation energies (corresponding to 0–0 vibronic transition) and we found that they are quite different for the calculation with and without PCM condition; B3LYP calculation estimated the adiabatic excitation energy for the neutral/anionic *p*-HBDI as 3.1 eV (399 nm)/2.81 eV (441 nm) without PCM, and as 2.74 eV (452 nm)/2.58 eV (480 nm) and 2.8 eV (443 nm) with PCM in methanol and THF, respectively. It should be noted that the 0–0 excitation energy is not corresponding to the peak position in spectra as existence of significant vibronic coupling. For the neutral *p*-HBDI, Table 1 shows

Table 2
Calculated and observed vertical excitation energies (eV) and corresponding oscillator strengths *f*1 and *f*2 for S_1 transition without and with PCM in methanol.

Method	ΔE/eV (nm) without PCM	*f*1	Δ/eV (nm) with PCM	*f*2
Neutral *p*-HBDI				
Exp.	3.13(395) [9]		3.51(353) [13]	
TD-B3LYP[a]	3.45	0.7	3.31	0.8
MCSCF/MCQDPT [26]	2.88			
EOM-CCSD//RI-MP2 [27]	4.12	0.82		
SOS-CIS(D)//RI-MP2 [27]	3.83	1.10		
XMCQDPT2//DFT(PBE0) [27]	3.31	0.51		
INDO/S-CIS [31]	3.24			
SAC-CI [34]	3.33	0.735		
BLYP [35]	2.99	0.00		
B3LYP [35]	3.46	0.66		
SAOP [35]	3.20	0.94		
CASPT2//CASSCF [35]	3.58			
EOM-CCSD [35]	4.00			
NDDO-G [36]	3.47	1.13	3.43	1.12
Anionic *p*-HBDI				
Exp.	2.60(475) [9]		2.96(419) [16]	
Exp.	2.78 (446) [36]			
Exp. [17]	2.57		2.91	
TD-B3LYPa	3.06	1.0	2.95	1.08
TD-B3LYP [17]	2.59	0.0003		
CIS [26]	4.37			
EOM-CCSD//RI-MP2 [27]	3.10	1.25		
XMCQDPT2//DFT(PBE0) [27]	2.51	1.19		
CASPT2//CASSCF [30]	2.51		2.69 (in water)	
CASPT2//CASSCF [32]	2.672	0.35		
SAC-CI [34]	2.39	0.887		
BLYP [35]	2.89	0.77		
B3LYP [35]	3.09	0.92		
SAOP [35]	2.93	0.80		
EOM-CCSD [35]	3.04			
NDDO-G [36]	2.70	1.38	2.86	1.30

[a] The present calculations.

that mode ν_{16} with larger Huang–Rhys factor has the biggest vibration frequency about 1620 cm^{-1} (0.2 eV), thus peak position of spectrum may shift about 0.2 eV from its 0–0 excitation energy plus inhomogeneous broadening of solvent effect; while for the anionic *p*-HBDI, peak position of spectrum may shift about 1319 cm^{-1} (0.16 eV) without PCM and 1523 cm^{-1} (0.19 eV) with PCM from its 0–0 excitation energy plus inhomogeneous broadening of solvent effect, respectively. On the other hand, vertical excitation energy calculated at local minimum of ground state S_0 is larger than its corresponding adiabatic excitation energy, and sometime this vertical excitation energy is regarded as peak position of spectrum. This is held only when the certain vibronic mode with the largest Huang–Rhys factor has right vibration frequency, but this is not generally happening. Table 2 shows that the present calculation of the vertical excitation energy for the neutral/anionic *p*-HBDI and it is 3.45 eV/3.06 eV without PCM, and 3.31 eV/2.95 eV with PCM in methanol, respectively. This corresponds to pure excitation from HOMO to LUMO. The corresponding oscillator strength in the present calculation shows similar value 0.7/1.0 without PCM and 0.8/1.08 with PCM for the neutral/anionic *p*-HBDI, respectively. The present calculations for the vertical excitation energy and oscillator strength agree with the other calculations without and/or with PCM in literatures [17,24,26,27,31–36]. It is interesting to note that vertical excitation energies from calculations are higher (higher or lower) than that of experimental measurement for the neutral (anionic) *p*-HBDI as shown in Table 2. However, the present simulation from Franck–Condon factors in Eqs. (1) and (2) is based on adiabatic excitation energy as shown in Table 1 and it predicts more reliable peak position of spectrum than the vertical excitation energy does.

Absorption and fluorescence spectra of the neutral *p*-HBDI were simulated first using Franck–Condon method with consideration of inhomogeneous broadening of solvent effect [18–20], in which the adiabatic excitation energies (0–0 transition) and corresponding Huang–Rhys factors in Table 1 were utilized in Eqs. (1) and (2). Absorption spectrum of the neutral *p*-HBDI from experiment measured at room temperature T = 298 K in methanol–water (1/1 vol) exhibits absorption peak and width at 3.35 eV (370 nm) and 0.54 eV [15]. The other experiment measurements with various solvents exhibit the absorption peaks varied from 360 nm to 373 nm [13]. The present simulation for absorption was carried at T = 298 K, and the results in Figure 3b and c show absorption peak and width at 2.98 eV (416 nm) and 0.61 eV with PCM and at 3.26 eV (380 nm) and 0.51 eV without PCM. Fluorescence spectrum of the neutral *p*-HBDI from experiment measured at temperature T = 77 K in non H-bonding 2-methyl THF glasses solvent exhibit peak and width at 2.85 eV (434 nm) and 0.66 eV [16]. The present simulation for fluorescence was carried at T = 77 K, and the results in Figure 4b and c show fluorescence peak and width at 2.62 eV (474 nm) and 0.64 eV with PCM and at 2.93 eV (423 nm) and 0.54 eV without PCM. The second peak appeared in primary shoulder band of fluorescence spectrum was also reproduced by the present calculation. In order to compare the calculation with TD-DFT method, we carried out Hartree–Fock (HF) calculation for the ground S_0 state and configuration interaction singles (CIS) calculation for the first excited S_1 state using 6-31+G(d) basis set, and the spectral simulation shows absorption (fluorescence) peak as 276 nm (378 nm) which is far from corresponding experiment value 370 nm (434 nm) as depicted in Figures 3d and 4d. This indicates that the correlation interaction plays very important role for spectral simulation in the neutral *p*-HBDI. We have checked the present calculation with the other two more density functionals, namely B3LYP-35 and BH and HLYP, for spectral simulation with and without PCM environment, and the results are basically similar to the B3LYP calculation.

Then, we simulated the absorption spectrum of the anionic *p*-HBDI using Franck–Condon factors. We estimated that partial charges around oxygen atoms become more negative in the anionic *p*-HBDI form than in the neutral *p*-HBDI form. Therefore, we assume that different inhomogeneous broadening of solvent effect must be taken into account for the vibration modes related and unrelated to oxygen atoms. This fact can be seen from Table 1 where vibronic-coupling modes are almost unchanged for the neutral *p*-HBDI with and without PCM, while they are changed a lot for the anionic *p*-HBDI. Inhomogeneous broadening parameter for vibration modes unrelated to oxygen atoms is chosen the same as the neutral *p*-HBDI as 800 cm^{-1}, and it is chosen as 350 cm^{-1} for vibration modes related to oxygen atoms for the anionic *p*-HBDI. The adiabatic excitation energy (0–0 transition) and corresponding Huang–Rhys factors in Table 1 were utilized in Franck–Condon simulation in Eq. (1). The absorption spectrum of the anionic *p*-HBDI from experiment measured at room temperature T = 298 K in H-bonding methanol solvent exhibits absorption peak and width at 2.96 eV (419 nm) and 0.56 eV [16], and the other experiment measurement in methanol solvent exhibits absorption peak and width at 428 nm and 0.50 eV [13]. The present simulation was carried at T = 298 K, and the results are shown in Figure 5b and c for absorption peak and width at 2.73 eV (455 nm) and 0.56 eV with PCM in methanol and at 2.95 eV (421 nm) and 0.57 eV without PCM. An overall spectral intensity in Figure 5b and c is calculated by the intensity related oxygen-atom vibrations plus the intensity unrelated to the oxygen-atom vibrations multiplied the ratio of these two spectral widths.

4. Concluding remarks

We have demonstrated that the peaks and widths of absorption and fluorescence spectra of the neutral and anionic *p*-HBDI are determined by combination of three factors in Franck–Condon simulation; vibronic coupling distributions, adiabatic excitation energies and inhomogeneous broadening of solvent effect. The equilibrium geometries of ground and excited states simulated with and without PCM are almost same for the neutral *p*-HBDI, but quite different for the anionic *p*-HBDI form. This difference leads to difference of vibronic coupling distributions with and without PCM. However, adiabatic excitation energy is sensitive to choice of PCM with different solvents for both neutral and anionic *p*-HBDI. Including the inhomogeneous broadening in Franck–Condon factors, we finally reproduced the spectral peaks and widths for both absorption and fluorescence well.

Acknowledgements

This Letter is supported by National Science Council of the Republic of China under Grant No. 100-2113-M-009-005-MY3. We would like to thank the MOE-ATU Project of the National Chiao Tung University for support. L.Y. thanks support from visiting program in National Chiao-Tung University. The first two authors contributed equally to this paper.

References

[1] M. Ormö, A.B. Cubitt, K. Kallio, L.A. Gross, R.Y. Tsien, S.J. Remington, Science 273 (1996) 1392.
[2] K. Brejc, T.K. Sixma, P.A. Kitts, S.R. Kain, R.Y. Tsien, M. Ormö, S.J. Remington, Proc. Natl. Acad. Sci. USA 94 (1997) 2306.
[3] O. Shimomura, FEBS Lett. 104 (1979) 220.
[4] C.W. Cody, D.C. Prasher, W.M. Westler, F.G. Prendergast, W.W. Ward, Biochemistry 32 (1993) 1212.
[5] R.Y. Tsien, Annu. Rev. Biochem. 67 (1998) 509.
[6] R. Heim, D.C. Parsher, R.Y. Tsien, Proc. Natl. Acad. Sci. USA 91 (1994) 12501.

[7] G.H. Patterson, S.M. Knobel, W.D. Sharif, S.R. Kain, D.W. Piston, Biophys. J. 73 (1997) 2782.
[8] S.B. Nielsen, A. Lapierre, J.U. Andersen, U.V. Pedersen, S. Tomita, L.H. Andersen, Phys. Rev. Lett. 87 (2001) 228102.
[9] M. Chattoraj, Proc. Natl. Acad. Sci. USA 93 (1996) 8362.
[10] G. Bublitz, B.A. King, S.G. Boxer, J. Am. Chem. Soc. 120 (1998) 9370.
[11] L.H. Andersen, A. Lapierre, S.B. Nielsen, I.B. Nielsen, S.U. Pedersen, U.V. Pedersen, S. Tomita, Eur. Phys. J. D 20 (2002) 597.
[12] A.B. Cubitt, R. Hemi, S.R. Adams, A.E. Boyd, L.A. Gross, R.Y. Tsien, Trends Biochem. Sci. 20 (1995) 448.
[13] J. Dong, K.M. Solntsev, L.M. Tolbert, J. Am. Chem. Soc. 128 (2006) 12038.
[14] J. Dong, K.M. Solntsev, O. Poizat, L.M. Tolbert, J. Am. Chem. Soc. 129 (2007) 10084.
[15] K.M. Solntsev, O. Poizat, J. Dong, J. Rehault, Y. Lou, C. Burda, L.M. Tolbert, J. Phys. Chem. B 112 (2008) 2700.
[16] N.M. Webber, S.R. Meech, Photochem. Photobiol. Sci. 6 (2007) 976.
[17] K. Lincke, T. Solling, L.H. Andersen, B. Klærke, D.B. Rahbek, J. Rajput, C.B. Oehlenschlæger, M.A. Petersen, M.B. Nielsen, Chem. Commun. 46 (2010) 734.
[18] J.E. Cotting, L.C. Hoskins, M.E. Levan, J. Chem. Phys. 77 (1982) 1081.
[19] S.H. Lin, C.H. Chang, K.K. Liang, R. Chang, Y.J. Shiu, J.M. Zhang, T.S. Yang, M. Hayashi, F.C. Hsu, Adv. Chem. Phys. 121 (2002) 1.
[20] T. Petrenko, F. Neese, J. Chem. Phys. 127 (2007) 164319.
[21] T. Petrenko, O. Krylova, F. Neese, M. Sokolowski, New J. Phys. 11 (2009) 015001.
[22] B. Mennucci, C. Cappelli, C.A. Guido, R. Cammi, J. Tomasi, J. Phys. Chem. A 113 (2009) 3009.
[23] J. Guthmuller, B. Champagne, J. Chem. Phys. 127 (2007) 164507.
[24] R. Nifosi, Y. Luo, J. Phys. Chem. B 111 (2007) 14043.
[25] M.J. Frisch et al., Gaussian 09, Revisions, A.02, Gaussian, Inc., Wallingford, CT, 2009.
[26] V. Helms, C. Winstead, P.W. Langhoff, J. Mol. Struct. (Theochem) 506 (2000) 189.
[27] I.V. Polyakov, B.L. Grigorenko, E.M. Epifanovsky, A.I. Krylov, A.V. Nemukhin, J. Chem. Theory Comput. 6 (2010) 2377.
[28] S. Olsen, S.C. Smith, J. Am. Chem. Soc. 129 (2007) 2054.
[29] S. Olsen, S.C. Smith, J. Am. Chem. Soc. 130 (2008) 8677.
[30] P. Altoe, F. Bernardi, M. Garavelli, G. Orlandi, F. Negri, J. Am. Chem. Soc. 127 (2005) 3952.
[31] A. Matsuura, T. Hayashi, H. Sato, A. Takahashi, M. Sakurai, Chem. Phys. Lett. 484 (2010) 324.
[32] M.E. Martin, F. Negri, M. Olivucci, J. Am. Chem. Soc. 126 (2004) 5452.
[33] A.V. Nemukhin, B.L. Grigorenko, A.P. Savitsky, Acta Natur. 2 (2009) 25.
[34] A.K. Das, J.-Y. Hasegawa, T. Miyahara, M. Ehara, H. Nakatsuji, J. Comput. Chem. 24 (2003) 1421.
[35] C. Filippi, M. Zaccheddu, F. Buda, J. Chem. Theory Comput. 5 (2009) 2047.
[36] A.A. Voityuk, A.D. Kummer, M.-E. Michel-Beyerle, N. Rosch, Chem. Phys. 269 (2001) 83.